Ratcheting strain as a crack driving force for crack growth

J. Tong, L.-G. Zhao, B. Lin, C. Cornet
Department of Mechanical and Design Engineering, University of Portsmouth, UK
jie.tong@port.ac.uk

ABSTRACT. Ratcheting deformation has significant implications on material damage and fatigue life of components under service loading conditions. In this work, we explore the concept of ratcheting strain as a crack driving force in controlling crack growth, both time-independent and time-dependent, utilizing elasto-plastic, visco-plastic and crystal-plasticity constitutive models. The viscoplastic and the crystal-plasticity models were implemented in the finite element software ABAQUS via user-defined material subroutines. Both stress-controlled and strain-controlled experiments were carried out to obtain the material parameters necessary to calibrate the models. Characteristics of crack tip deformation were examined at room and elevated temperature for both stationary and growing cracks using the finite element method. Whilst the strain range and the stress range remained stable throughout the cycles, distinctive strain ratcheting behaviour near the crack tip was captured in all cases, leading to progressive accumulation of tensile strain normal to the crack growth plane. It is possible that this tensile strain, or ratcheting strain, may be responsible for material separation leading to crack growth. Results show also that low frequencies and superimposed hold periods at peak load significantly enhanced strain accumulation near the crack tip. Application of a criterion based on ratcheting strain in the prediction of crack growth at elevated temperature was also attempted.

KEYWORDS. Crack tip; Constitutive behaviour; Ratcheting; Fatigue crack growth.

INTRODUCTION

For decades fatigue crack growth rates have been correlated with elastic stress intensity factor ranges in small scale yielding situations with considerable success. However, efforts at relating micro-structural models of material separation to continuum deformation analyses have so far not been very successful [1, 2]. The situation is changing rapidly though, with the development of more accurate material constitutive models, the drastic increase in computing power and the advance of powerful experimental tools such as synchrotron X-ray. A fundamental understanding of the physical processes associated with fatigue crack growth may finally be approached.

We reported in 2004 an incidental observation of ratcheting strain development near a crack tip during a study of crack closure [3], using an elastic-plastic constitutive model in ABAQUS that includes simple terms of kinematic and isotropic hardening. Whilst the stress and the strain ranges remained essentially unchanged throughout the cycles and scaled with the external load range, progressive accumulation of tensile strains occurred near the crack tip. We extended this work in recent years to consider viscoplastic material behaviour for growing cracks as well as stationery cracks [4]. Stress-controlled, as well as strain-controlled, experiments were carried out to calibrate the material parameters, with an additional kinematic hardening term introduced to regulate the development of the uniaxial ratcheting strains [5]. Again ratcheting behaviour was observed near the crack tip, which appears to be only weakly dependent of the particular constitutive formulation. More recently, a crystal-plasticity model [6] was also used to examine the near-tip deformation characteristics, again, similar ratcheting behaviour was also observed. This paper aims to present some of the key findings

from the above work, as well as further evidence from our most recent work, which appear to favour the concept of a ratcheting strain as a crack driving force in controlling near-tip material separation.

THE MATERIALS MODELS

Chaboche Unified Constitutive Model

The material model used in [4, 5] is essentially the unified constitutive equations by Chaboche [7], where both isotropic (R) and kinematic (α) hardening variables are considered during the transient and saturated stages of cyclic response. The inelastic strain $\boldsymbol{\varepsilon_p}$ represents both plastic and creep strains. A power relationship is adopted for the viscopotential and the viscoplastic strain rate is expressed as [7]:

$$\dot{\varepsilon}_p = \left\langle \frac{f}{Z} \right\rangle^n \frac{\partial f}{\partial \sigma} \tag{1}$$

where f is the yield function, $\boldsymbol{\alpha}$ is the back stress or kinematic hardening variable, Z and n are material constants. According to the von Mises yield criterion, the yield function f is defined as

$$f(\sigma,\alpha,R,k) = J(\sigma-\alpha) - R - k \le 0 \tag{2}$$

where R is the isotropic hardening variable and k is the initial value of the radius of the yield surface. J denotes the von Mises distance in the deviatoric stress space

$$J(\sigma-\alpha) = \sqrt{\frac{3}{2}(\sigma'-\alpha'):(\sigma'-\alpha')} \tag{3}$$

where $\boldsymbol{\sigma'}$ and $\boldsymbol{\alpha'}$ are the deviators of $\boldsymbol{\sigma}$ and $\boldsymbol{\alpha}$, : represents the inner product of two tensors. Plastic flow occurs under the condition $f = 0$ and $\frac{\partial f}{\partial \sigma} : \dot{\sigma} > 0$.

The evolution of the kinematic stress tensor $\boldsymbol{\alpha}$ and the isotropic stress R may be described as [7]:

$$\begin{cases} \dot{\alpha} = \dot{\alpha}_1 + \dot{\alpha}_2 \\ \dot{\alpha}_1 = C_1(a_1\dot{\varepsilon}_p - \dot{\alpha}_1\dot{p}) \\ \dot{\alpha}_2 = C_2(a_2\dot{\varepsilon}_p - \dot{\alpha}_2\dot{p}) \end{cases} \quad \text{and} \quad \dot{R} = b(Q-R)\dot{p}\,, \tag{4}$$

where C_1, γ_1, C_2, γ_2, b and Q are material and temperature dependent constants which determine the shape and amplitude of the stress–strain loops during the transient and saturated stage of cyclic response, and $\dot{p}$ is the accumulated inelastic strain rate defined by

$$\dot{p} = \left\langle \frac{f}{Z} \right\rangle^n = \sqrt{\frac{2}{3} d\dot{\varepsilon}_p : d\dot{\varepsilon}_p} \tag{5}$$

The constitutive equations contain eleven material parameters, namely, E, ν, k, b, Q, C_1, a_1, C_2, a_2, Z and n. These were calibrated using the uniaxial strain-controlled and stress controlled experimental data at 650°C [5]. The above material model has been implemented in ABAQUS via a user defined material subroutine (UMAT).

Crystal Plasticity Model

The framework of crystal plasticity theory used in [6] was based on the multiplicative decomposition of the total deformation gradient $\boldsymbol{F}$ into an elastic ($\boldsymbol{F^e}$) part and a plastic ($\boldsymbol{F^p}$) part [8]. The plastic component $\boldsymbol{F^p}$ is calculated from the inelastic velocity gradient $\boldsymbol{L^p}$ according to:

$$L^p = \dot{F}^p F^{p^{-1}} = \sum_{\alpha=1}^{n} \dot{\gamma}^\alpha (m^\alpha \otimes n^\alpha) \tag{6}$$

where $\dot{\gamma}^{\alpha}$ is the shear strain rate on the slip system α, m^{α} and n^{α} are the slip direction and the slip plane normal, respectively.
With the incorporation of two scalar state variables per slip system, i.e., slip resistance (S^{α}) and back stress (B^{α}), the flow rule is expressed as an exponential function of the resolved shear stress on the slip system [9]:

$$\dot{\gamma}_{\alpha} = \dot{\gamma}_0 \exp\left[\frac{-F_0}{\kappa\theta}\left\langle 1-\left\langle\frac{\left|\tau^{\alpha}-B^{\alpha}\right|-S^{\alpha}\mu/\mu_0}{\hat{\tau}_0\mu/\mu_0}\right\rangle^{p}\right\rangle^{q}\right]\mathrm{sgn}(\tau^{\alpha}-B^{\alpha}) \tag{7}$$

where κ is the Boltzmann constant, τ^{α} is the resolved shear stress on the slip system α, θ the absolute temperature, μ and μ_0 the shear moduli at θ and 0 Kelvin, respectively, and F_0, $\hat{\tau}_0$, p, q and $\dot{\gamma}_0$ are material constants. The two internal variables, the slip resistance in each slip system, S^{α}, and the back stress, B^{α}, are introduced. The slip resistance on a generic slip system is assumed to evolve according to:

$$\dot{S}^{\alpha} = \left[h_S - d_D(S^{\alpha}-S_0^{\alpha})\right]\left|\dot{\gamma}^{\alpha}\right| \tag{8}$$

where the first and second terms are static and dynamic recovery terms associated with the material constants h_S and d_D, respectively.
The back stress evolves according to a standard hardening-dynamic recovery format [9],

$$\dot{B}^{\alpha} = h_B\dot{\gamma}^{\alpha} - r_D B^{\alpha}\left|\dot{\gamma}_{\alpha}\right| \tag{9}$$

where h_B is a hardening constant, and r_D is a dynamic recovery function which may be expressed as:

$$r_D = \frac{h_B\mu_0}{S^{\alpha}}\left\{\frac{\mu_0'}{f_c\lambda}-\mu\right\}^{-1} \tag{10}$$

where f_c is a coupling parameter between the internal slip variables and μ_0' the local slip shear modulus at 0 Kelvin.
The crystallographic formulation was implemented into ABAQUS (2009) within the framework of large strain kinematics via a user-defined material subroutine (UMAT). The material constants were calibrated using the same set of experimental data as that in [5].

THE FINITE ELEMENT PROCEDURES AND RESULTS

Viscoplasticity Analyses

A standard CT specimen [4] and a single edge tension (SENT) [5] specimens were meshed using four-node, first-order elements with full integration. The element size near the crack tip is 12.7 μm, about twice the average grain size (5~6 μm) of the material. For consistency, the same mesh was used to analyse the crack tip deformation for both stationary and growing cracks. For stationary crack analysis, the crack length was chosen to be a = 13mm, a/W = 0.5 for CT; a = 3.5mm, a/W = 0.354 for SENT, respectively. For growing crack analysis, a total crack growth of 1.2 mm was simulated. For CT specimen, finite element computations were carried out over 30 cycles at selected load ratios with a maximum external load of 7kN and a frequency of 0.5 Hz, conditions chosen to simulate a typical crack growth rate of 5×10^{-7} m/cycle. The stress-strain loops (in the y-direction) at a Gauss integration point just ahead of the crack tip (r = 3.8μm, θ ≈ 45°) are shown in Fig.1 for a constant load range of 7 kN and load ratios of R = 0 and 0.3. More pronounced strain accumulation occurs at R = 0.3, compared with R = 0; although, for both cases, the stress and the strain ranges remain almost constant and scale with the applied load range for each successive cycle. The same behaviour was also observed in the SENT specimen, where the mean ratcheting strain is found to increase with the number of cycles, whilst the ratcheting strain increment decreases with the number of cycles although no shakedown occurs. A similar behaviour was observed for a growing crack, where ratcheting is clearly visible as the crack approaches the observation point C, as shown in Fig. 2.

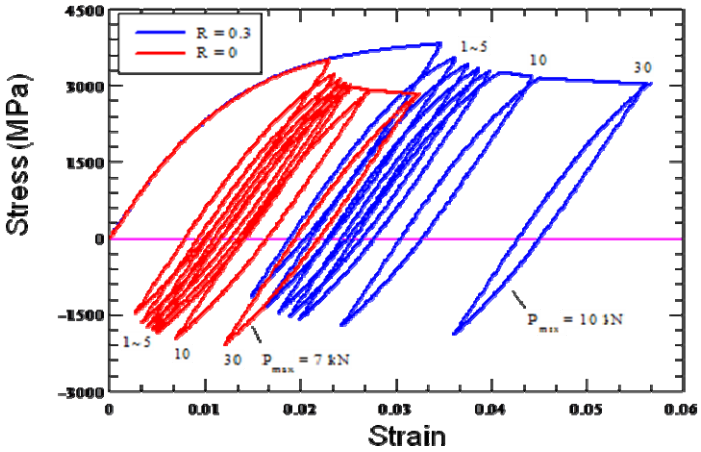

Figure 1: The evolution of stress–strain loops over 30 cycles at a Gauss integration point ahead of the crack tip (r = 3.8μm, θ ≈ 45°) for load ratios R = 0.3 and 0, ΔP = 7kN [4].

The change of the local strain and stress ranges with the number of cycles has been examined for selected loading frequencies and dwell periods. Irrespective of the loading conditions, the strain and the stress ranges remain mostly unchanged (within 2-3%) with the number of cycles. The local stress ratios, however, are very different from the remote applied load ratios due to the evolution of hysteresis inelastic deformation near the crack tip. Significantly lower, mostly negative, stress ratios present near the crack tip, irrespective of the applied load ratio, although how this change affect the crack growth is still unknown. Contrary to the relative constant stress/strain ranges and negative stress ratio, the near-tip strain component perpendicular to the crack plane increases with the decrease of the loading frequency and the increase of the dwell period. This seems to suggest that strain accumulation is a plausible mechanism for crack growth.

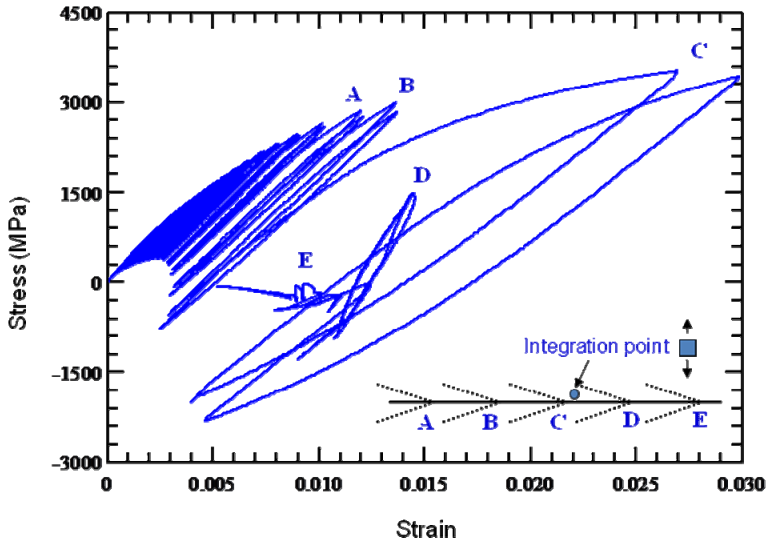

Figure 2: The evolution of stress-strain loops at an integration point O ahead of a growing crack. The distances to the growing crack tip are: AO = 29.2 μm, BO = 16.5 μm, CO = 3.8 μm [4].

Crystal Plasticity Analyses

The near-tip stress-strain responses have been examined using a crystal-plasticity constitutive model. A standard CT specimen was meshed, as in [4]; whilst a submodel was constructed near the crack tip and contains 150 grains with randomly assigned orientations. The loading was prescribed by the displacement of its boundaries from the global viscoplastic analyses. A transgranular crack across a couple of grains (18 μm) was introduced in the submodel, with some of the grains in the vicinity of the crack tip identified in the inverse pole figure (Fig. 3a). The model parameters were

calibrated using the same set of experimental data as that used in [4, 5]. The model was utilised to study the near-tip micromechanics behaviour and the influence of localized stress and strain concentrations due to the microstructure effect. Fig. 3 shows a similar stress-strain response from the viscoplastic and the crystal-plastic model, where ratcheting can be observed for both cases. For a given location near the crack tip, Grain 1, for example, the actual stress-strain response appears to be dependent on the grain orientation, with more ratcheting developed in a "soft" grain (Grain 1s) than in a "hard" grain (Grain 1h), as shown in Fig. 3b.

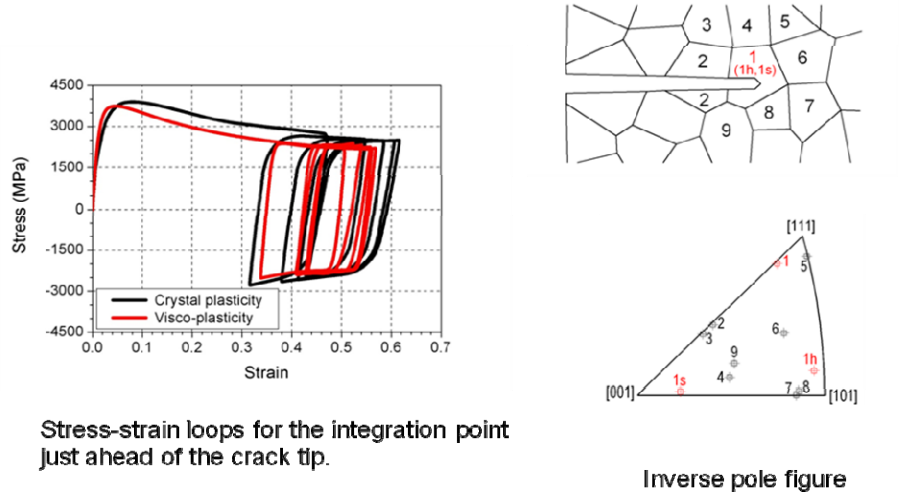

Figure 3: (a) Comparison of the viscoplastic and the crystal-plastic model responses, with the crack tip and Grain 1 identified. The orientations of Grain 1 were assigned artificially to obtain a "hard" (1h) and a "soft" (1s) grain, as shown in the pole figure. (b) The stress-strain responses from the crystal-plasticity model for the "hard" and the "soft" grain, ratcheting noted in both cases.

Applications

We hypothesise that a crack starts to propagate when the ratcheting strain at a characteristic distance to the crack tip reaches a critical value. This criterion may be used to predict crack growth rates. In this work, the number of cycles was recorded when the ratcheting strain reached a critical value over a characteristic distance $d^* = 12.7\mu m$ ahead of the crack tip. This critical value was back calculated using the finite element analysis to predict the same crack growth rate as that obtained experimentally. The average crack growth rate was then calculated by dividing the characteristic distance with the recorded number of cycles. Using the proposed criterion, crack growth rates were predicted from the finite element analyses of the SENT geometry for dwell loading conditions with a load ratio $R = 0.1$, where a dwell period of 1s, 30s and 300s was superimposed on the maximum load, and the results are shown in Fig. 4. These predicted results show a very similar trend to that obtained from tests in vacuum, where the influence of oxidation is removed hence viscoplastic deformation alone controls the crack growth.

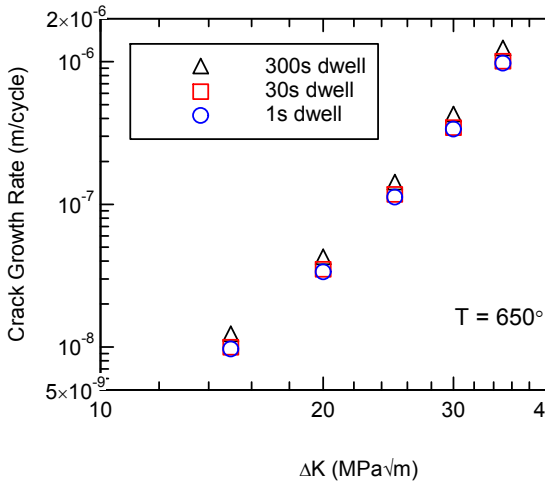

Figure 4: Predicted crack growth rates against ΔK for selected dwell periods, viscoplastic model.

DISCUSSION

The role of a characteristic length in fracture and fatigue has been explored since the 60s. McClintock [10, 11] developed a mechanistic analysis of crack extension by fatigue. He employed an anti-plane shear perfect plasticity solution and a failure criterion based on plastic strain accumulation over a "structural size" of the material. McClintock's studies provided a framework for tensile crack growth in ductile materials, particularly with regard to micro-mechanisms resulting in material separation. Quantitatively, a structural size of 5μm was found to fit well with the experimental results for the three materials examined [11]. A criterion for crack growth in elastic-plastic materials was phrased in terms of critical conditions that exist over a characteristic distance [12, 13]. Krafft [14] proposed that ductile fracture would occur when a critical strain for a uniaxial tensile specimen is achieved at the crack tip over a distance equal to the spacing of void nucleating particles. Ritchie et al. [13] successfully predicted fracture when a critical stress was achieved over two grain sizes; similarly in Rawal and Gurland [15] over a critical distance about 1.3 grain-sizes. The choice of characteristic distance introduces a physical length scale associated with the fracture process, thus avoiding issues associated with the stress/strain singularity ahead of a crack tip. In the present work, for convenience, the chosen distance d^* corresponds to the dimension of one element (12.7μm) ahead of the crack tip in the finite element mesh, which is also about twice an average grain size of the material. This characteristic length of about the size of 1 to 2 grains is important, as further afield mean strains perpendicular to the crack plane decrease with the number of cycles, as shown in Fig. 4; whilst too close to the crack tip where large deformation predominates, similar reduction of strain with cycle also occurs [4]. A ratcheting strain of 4.7% over d^*=12.7μm was used as a crack growth criterion in [4], which is also close to the failure strain of the material from uniaxial ratcheting testing [5].

The crack growth criterion proposed in the current work is essentially a strain-based approach, which has been widely used for prediction of viscoplastic failures such as creep [16]. The strains local to a crack tip are of multiaxial nature such that an equivalent strain, which accounts for all strain components, is often adopted as a damage parameter [16, 17]. In the current work, however, only the strain component normal to the crack growth plane was considered, as it is most relevant to material separation in mode I, and it also coincides with the maximum principal strain [18]. The choice of failure criterion may depend on the material constitutive behaviour, as proposed by Kapoor [19, 20]. Two modes of failure may be identified in ductile rupture: low cycle fatigue (LCF) and ratcheting. According to Kapoor, if a strain cycle is closed, then failure takes place by low cycle fatigue; while if a strain cycle is open, tensile strain will develop and failure by ratcheting will occur. Ratcheting occurs when the accumulated strain reaches a critical value, which may be comparable with the strain to failure in a monotonic test. LCF and ratcheting failure are competitive independent failure mechanisms, and whichever corresponds to an earlier failure governs the life of the specimen. In the current work, the value of the critical strain was chosen based on the baseline experimental results, subsequently used to predict the crack growth rates for other conditions. A critical ratcheting strain of ~5% at 650°C would seem to be adequate in the prediction of crack growth in this material. The fact that the ratcheting strain criterion predicts reasonably well the effect of frequency and dwell time on crack growth rate is encouraging. Although ratcheting has been used as a failure criterion

in wear-related studies [19, 20], this is the first time the concept is used for the prediction of fatigue crack growth in time-independent [3] and time-dependent [4, 5] situations.
We have since found that ratcheting strains scale generally with accumulated plastic strains over a given cyclic period, and they compare particularly well at large strains. Hence both ratcheting strain and accumulated plastic strain may be used in the crack growth criterion.

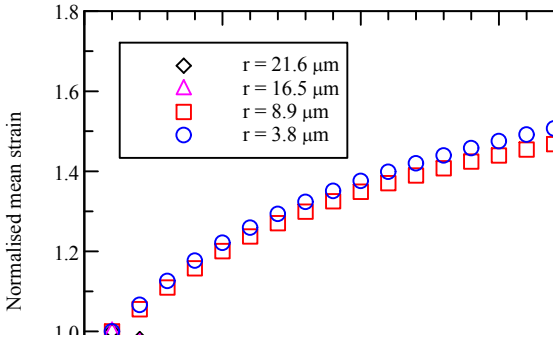

Figure 4: Normalised mean ratcheting strain at selected distance to the crack tip as a function of number of cycles.

ACKNOWLEDGEMENTS

The authors gratefully acknowledge the support of TSB (DISPLACE) and EPSRC (EP/E062180/1; EP/E05658X/1) during the course of this work. The crystal plasticity UMAT was originally developed by Professor Esteban Busso and his associates while he was with the Imperial College, London.

REFERENCES

[1] J. R. Rice, In: Fatigue Crack Growth, ASTM STP 415 (1967) 247.
[2] P. C. Paris, Fatigue Fract. Engng. Mater. Struct., 21 (1998) 535.
[3] L.-G. Zhao, J. Tong, J. Byrne, Fatigue Fract. Engng. Mater. Struct., 27 (2004) 19.
[4] L.-G. Zhao, J. Tong, J Mech. Physics Solids, 56 (2008) 3363.
[5] C. Cornet, L.-G. Zhao, J. Tong, Eng. Fract. Mech., 76 (2009) 2538.
[6] B. Lin, L.G. Zhao, J. Tong, Eng Fract Mech., under review.
[7] J. L. Chaboche, Int. J. Plasticity, 5 (1989) 247.
[8] R. J. Asaro, Applied Mechanics 23 (1983) 1.
[9] E.P. Busso, F. T. Meissonnier, N. P. O'Dowd, J. Mech. Physics Solids, 48 (2000) 2333.
[10] F.A. McClintock, In: Fracture of Solids, John Wiley & Sons Inc., New York, USA (1963).
[11] F.A. McClintock, G.R. Irwin, In: Fracture Toughness Testing and Its Applications, ASTM STP 381 (1965) 84.
[12] F.A. McClintock, ASME J Applied Mechanics, 25 (1958) 582.
[13] R.O. Ritchie, J.F. Knott, J.R. Rice, J. Mech. Physics of Solids, 21 (1973) 395.
[14] J.M. Krafft, Applied Materials Research, 3 (1964) 88.
[15] S.P. Rawal, J. Gurland, Metall. Trans. A, 8 (1977) 691.
[16] H. Riedel, J.R. Rice, In: Tensile cracks in creeping solids, ASTM STP 700 (1980) 112.
[17] R.O. Ritchie, A.W. Thompson, Meta. Trans. A, 16 (1985) 236.
[18] Z. Qian, S. Takezono, K. Tao, Int. J. Solids and Structures, 33m (1996) 3601.
[19] A. Kapoor, K.L. Johnson, Proc. R. Soc. Lond. A, 445 (1994) 367.
[20] A. Kapoor, Wear, 212 (1997) 119.